Next Materials 9 (2025) 101040

Contents lists available at ScienceDirect

Next Materials

journal homepage: www.sciencedirect.com/journal/next-materials

Research article

High temperature photoluminescence sensitivity of Te^{4+} in silver nanoparticle tellurite glasses: Application as optical temperature sensor

Adriana do Carmo Capiotto [a], Luis Humberto da Cunha Andrade [a], Junior Reis Silva [a], Luiz Antonio de Oliveira Nunes [b], Sandro Marcio Lima [a,*]

[a] Programa de Pós-Graduação em Recursos Naturais (PGRN), Centro de Estudos em Recursos Naturais (CERNA), Universidade Estadual de Mato Grosso do Sul (UEMS), C.P. 351, Dourados, MS, Brazil
[b] Instituto de Física de São Carlos (IFSC), Universidade de São Paulo (USP), São Carlos, SP, Brazil

ARTICLE INFO

Keywords:
Te^{4+} semi metal ion
Tellurite glass
Photoluminescence
Optical temperature sensor
Relative sensitivity

ABSTRACT

Tellurite glasses with the composition (in mol%) (100-x)($75TeO_2$:$25Li_2O$):x$AgNO_3$ (x = 0, 0.6, and 1.2) were synthesized at 800 °C in an ambient atmosphere, for investigation of the influence of Ag nanoparticles on the Te^{4+} semi metal ion photoluminescence ($^3T_{1\ u} \rightarrow {}^1A_{1\ g}$ transition). The temperature dependence of the Te^{4+} emission was evaluated, aiming at application of the glass as an optical temperature sensor. A structural investigation of the samples was performed using X-ray diffractometry and Raman spectroscopy. The UV-Vis optical characteristics of the materials were determined by absorption, photoluminescence, photoluminescence excitation, and lifetime measurements. The sensitivity of the optical temperature measurement was determined based on the parameters emission lifetime, photoluminescence excitation intensity, and photoluminescence intensity ratio. The results showed that the silver nanoparticles increased the Te^{4+} PL intensity in the red region. For optical temperature sensing, a decrease in the Te^{4+} PL intensity, combined with a blue shift, occurred when the temperature was increased from ambient to 353 K, resulting in a maximum relative sensitivity of 3.7 %/K at room temperature. This high sensitivity indicated the suitability of the tellurite system as a potential candidate for application as an optical temperature sensor.

1. Introduction

In the last few years, there has been an intensified search for temperature sensors that do not require mechanical contact with the test body during the measurement. In particular, sensors based on the optical properties of a luminescent material offer advantages when it is desired to monitor the temperatures of, for example, corrosive media or environments with high electromagnetism. Other benefits of non-contact optical temperature sensors are that they provide fast and accurate responses, with excellent stability, sensitivity, and spatial resolution [1].

The temperature dependence of the luminescence signal can be monitored in different ways, such as by its intensity, spectral shape and bandwidth, or lifetime [1–8]. An ideal material is one that exhibits a substantial change in luminescence according to a small temperature variation, ensuring high sensitivity. It is also desirable to be able to determine the temperature dependence of the luminescence signal in the simplest possible way, preferably using a single excitation and a single emission measurement, enabling rapid evaluation of relative sensitivity. For this purpose, the temperature dependence of the lifetime has been most commonly used.

Various materials doped with rare earths (REs) have been investigated as candidates for luminescent temperature sensors, mainly using Eu^{3+}, Sm^{3+}, Nd^{3+}, and Tb^{3+} [8–13]. The combined absorption and emission characteristics of REs, together with their high luminescence quantum efficiencies, make them good candidates for use in temperature sensors. However, some luminescent transition metals and semi metals have also attracted interest, because their strong interactions with the matrices in which they are inserted result in more pronounced luminescence thermal quenching, which is an important characteristic for a thermal sensor [3].

Tellurite glasses, based on tellurium dioxide (TeO_2), have garnered significant research interest due to their optical properties, such as, a high refractive index (typically ranging from 1.9 to 2.3 in the visible region), a wide optical transparency window extending from the near-ultraviolet to the mid-infrared (approximately 0.3–5 μm), and a relatively low phonon energy (~700 cm^{-1})[14]. These characteristics have

* Corresponding author.
E-mail address: smlima@uems.br (S.M. Lima).

https://doi.org/10.1016/j.nxmate.2025.101040
Received 20 March 2025; Received in revised form 3 July 2025; Accepted 1 August 2025
Available online 6 August 2025
2949-8228/© 2025 The Authors. Published by Elsevier Ltd. This is an open access article under the CC BY-NC license (http://creativecommons.org/licenses/by-nc/4.0/).

spurred investigations into their potential as host materials for various luminescent ions, particularly REs elements. The inherent advantages of tellurite glasses, including their relatively low melting point and facile preparation techniques, facilitate the incorporation of REs at high doping concentrations, enabling the development of a wide range of optical devices, such as optical temperature sensor.

Recent work has reported high luminescence quantum efficiency (0.63 ± 0.06) at room temperature for the Te^{4+} semi metal ion in tellurite glass, under UV-blue excitation [15,16]. This behavior is influenced by the ns^2 type electronic configuration (of Te^{4+}, Sn^{2+}, and Sb^{3+}, for example), which can vary with the coordination field, due to the presence of electrons in the outermost layer. Other effects are related to the chemical composition of the glass network and the cooling process [17]. Because of this interesting discovery, our research group has explored the factors that influence Te^{4+} formation in tellurite glass [18, 19] and how the Te^{4+} emission in this glass can be used for different photonic applications [20,21]. The studies indicated that a fraction of the TeO_2 used to synthesize the glass was present in the Te^{4+} electronic configuration, with the concentration being dependent on the modifier (Li_2O) concentration, melting temperature, and atmosphere [22].

It is well known that the incorporation of metallic nanoparticles (NPs) in glasses favors increased UV-Vis absorption by some RE ions, resulting in enhanced emission intensity [23–27]. Therefore, to further improve the absorption and emission of Te^{4+} in tellurite glass, a binary system was prepared using a TeO_2:Li_2O ratio of 75:25 (in mol%), with silver nanoparticles (AgNP) as dopant, and a full spectroscopic investigation was performed. The temperature dependence of the Te^{4+} photoluminescence in the glass host was evaluated, with determination of the relative sensitivity using the emission lifetime, photoluminescence excitation intensity, and photoluminescence intensity ratio. The results indicated that the use of AgNP in preparation of the glass substantially improved its optical properties, making it an excellent candidate for use in optical temperature sensing applications.

2. Materials and methods

Tellurite glasses (here denoted TL) with the composition (in mol%) (100-x)(75 %TeO_2:25 %Li_2O):x$AgNO_3$ (x = 0, 0.6, and 1.2 mol%) were synthesized at a melting temperature of 800 °C, in an ambient atmosphere. The powders were macerated in an agate mortar for 30 min, placed in a platinum/gold (95 %Pt/5 %Au) crucible, and heated in an oven (Press2–52/0912, EDG) at a rate of 10 °C/min until reaching 400 °C, maintained for 1 h, followed by further heating at a rate of 10 °C/min up to the melting temperature of 800 °C, maintained for 1 h. An annealing treatment was performed during 5 h in a stainless steel mold preheated to 270 °C. After this procedure, the samples were cut and polished, resulting in thicknesses of 0.81, 0.67, and 0.81 mm for the TL:Te^{4+}, TL:Te^{4+}/0.6Ag, and TL:Te^{4+}/1.2Ag materials, respectively.

Raman scattering was performed with a 45 mW laser, at a wavelength of 532 nm. The signal was recorded using a confocal microscope (BX51 – Voyage) coupled to a monochromator (Andor) and a charge-coupled device (CCD) detector. X-ray diffraction measurements were performed using a Miniflex-500 diffractometer (Rigaku).

UV/Vis/NIR absorption spectra were acquired in the range 350–900 nm, using a LAMBDA 1050 spectrophotometer (PerkinElmer). The emission lifetime of Te^{4+} was obtained with excitation at 375 nm, using an optical parametric oscillator (Vibrant LD 355, Opotek) coupled to a Nd^{3+}:YAG laser (10 Hz) operated with pulse duration of 10 ns. Photoluminescence (PL) spectra were acquired using a diode laser (OBIS, Coherent) operated at 375 nm, with signal detection by a high sensitivity spectrometer (Maya 2000, Ocean Optics).

The samples were evaluated as optical temperature sensors in different ways: (1) by observing the Te^{4+} lifetime; (2) using photoluminescence excitation (PLE); and (3) using the ratio between the wavelength corresponding to the peak and the maximum PL intensity. For each method, the relative sensitivity (S_r) was determined. The temperature dependence of PL and PLE (from 298 to 353 K) was determined using a fluorimeter (LS55, PerkinElmer) with a pulsed Xe lamp source. During the measurement, the sample was fixed in a custom-built heating system fitted with a type E thermocouple and a temperature controller (331S, Lake Shore). The photoluminescence was registered after sample and sample holder are in thermal equilibrium.

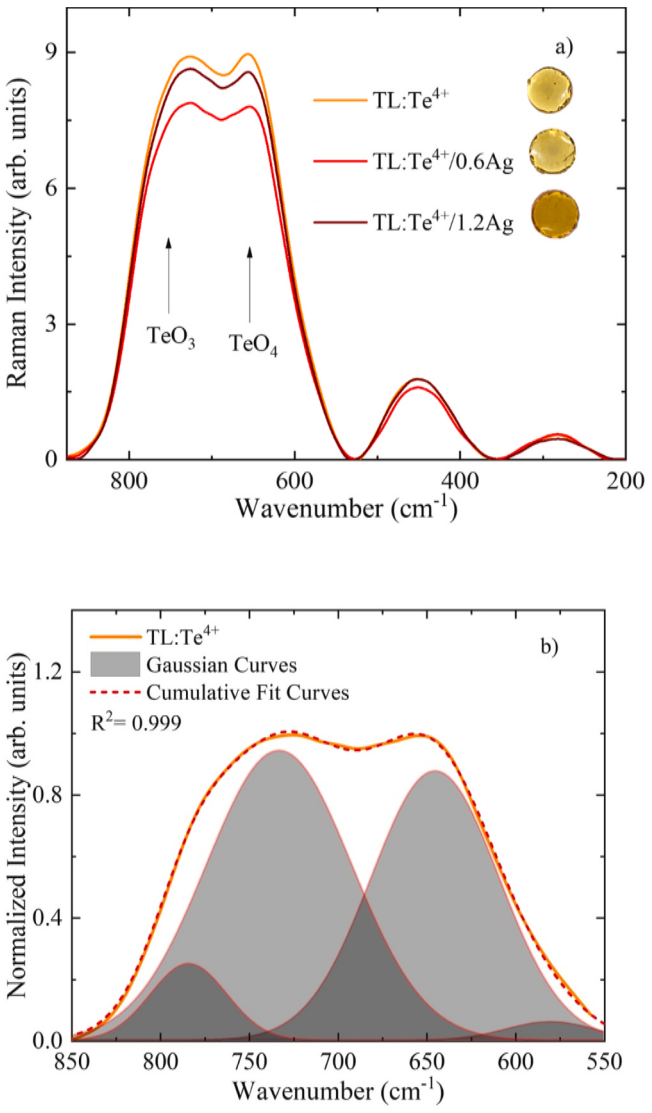

Fig. 1. **(a)** Raman spectra of the TL:Te^{4+}/Ag glasses in the range from 200 to 900 cm^{-1}. **(b)** Raman spectrum of the TL:Te^{4+} glass in the range from 550 to 850 cm^{-1}, Gaussian function deconvolution (gray shading), and sum of the peaks (red dashed line).

3. Results and discussion

3.1. Structural investigation

Structural analyses employed X-ray diffraction and Raman spectroscopy, mainly to examine the effect of AgNP on the glass morphology. The X-ray diffractograms of the glasses revealed amorphism, showing the presence of non-crystalline phases.

Raman spectra were acquired between 200 and 900 cm^{-1}, with the main vibrational modes (Fig. 1(a)) showing strong similarity among the samples, indicating that the presence of a low concentration of AgNP did not affect the Te^{4+} in the glass. The scattering observed in the 200–370 cm^{-1} interval could be attributed to the vibration of TeO_3 in a

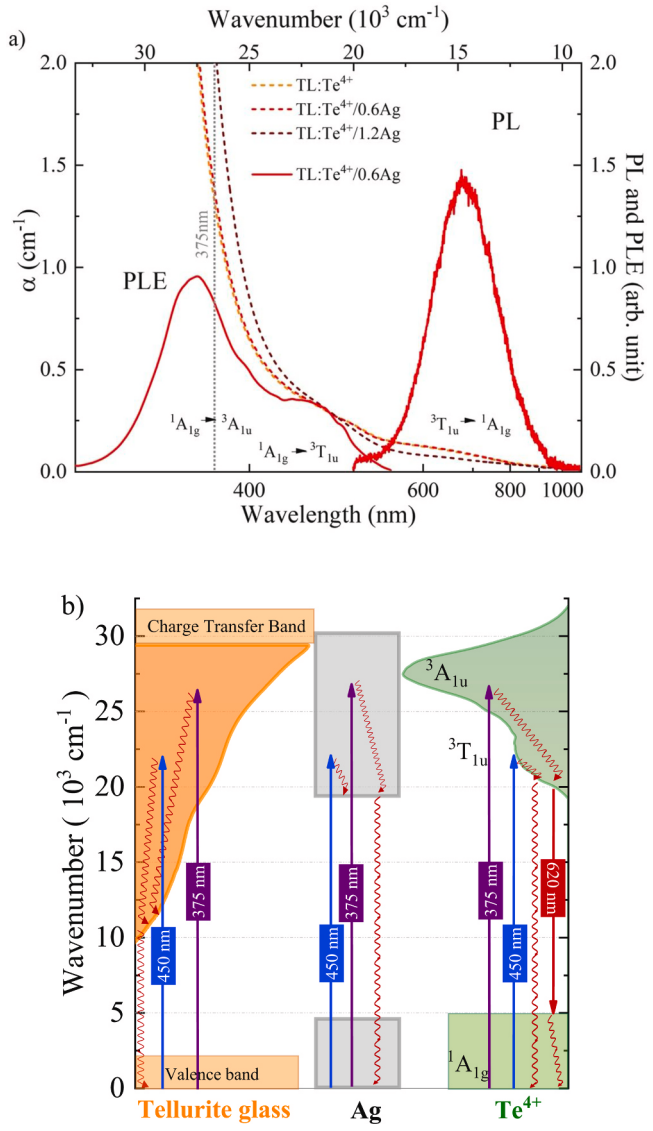

Fig. 2. (a) Absorption coefficient spectra for the three studied glasses, together with (for the TL:Te^{4+}/0.6Ag glass) the photoluminescence (PL) spectra obtained with excitation at 375 nm and the photoluminescence excitation (PLE) spectra in the range from 300 to 550 nm (observing the emission at 620 nm). **(b)** Schematic energy level diagram for the studied tellurite system, indicating the absorption regions for the glass, Ag, and Te^{4+}. The solid arrows show the radiative transitions (absorption and emission) and the wavy red lines indicate the nonradiative transitions.

trigonal pyramidal (tp) configuration with two or three non-bridging oxygen (NBO) atoms [18,19,28]. Scattering in the 370–530 cm^{-1} interval was due to symmetric stretching of Te–O–Te in the vertices of trigonal bipyramidal (tbp) TeO_4, as well as the TeO_{3+1} polyhedron and tp TeO_3. Broad bands between 530 and 900 cm^{-1} could be ascribed to the continuous TeO_4 tbp cells. At around 790 cm^{-1}, there was the influence of the Te and NBO present in the TeO_{3+1} polyhedron or in the tp TeO_3 [29]. The pairs of free electrons in tellurium led to the formation of short and long equatorial bridges of Te–O–Te, with bands at around 640 cm^{-1} corresponding to asymmetric stretching in the TeO_4 tbp units [30,31]. A band at 730 cm^{-1} could be attributed to stretching vibration between Te and NBO [32].

The structural similarity among the samples was confirmed by deconvolution of the Raman spectra in the range 550–850 cm^{-1}, with four Gaussian curves centered at 590, 640, 730, and 790 cm^{-1}. As an example, Fig. 1(b) shows the cumulative fit curve and the Gaussian deconvolution for the TL:Te^{4+} glass. The Gaussian areas were determined for each spectrum and the Te–O coordination numbers ($N_{Te\text{-}O}$ ~3.45) and NBO values (~0.35) were calculated using models reported in the literature [33–36]. The values obtained were the same for all the tellurite glasses, independent of the AgNP concentration, further corroborating the preservation of the glass structure when AgNP was incorporated in the matrix.

The minor variations in overall Raman intensity observed between samples (Fig. 1a) can be attributed to experimental factors such as slight differences in sample positioning, surface quality, and thickness, rather than fundamental structural changes. This is confirmed by the consistent peak positions and relative band intensities across all samples. The incorporation of silver at these low concentrations (0.6–1.2 mol%) does not significantly alter the tellurite network structure, as evidenced by the identical Te-O coordination numbers (~3.45) and NBO values (~0.35) across all samples. This structural preservation indicates that silver ions and nanoparticles likely occupy interstitial positions within the glass network without disrupting the Te^{4+} environments responsible for the observed luminescence properties. The consistent Raman profiles confirm that the enhanced luminescence observed with increasing silver content is due to plasmonic interactions rather than structural modifications of the Te^{4+} centers.

3.2. Optical spectroscopy investigation

The UV-Vis absorption and emission characteristics of the tellurite glasses were determined to elucidate the effects of the presence of Te^{4+} ions and AgNP in the glass. Fig. 2(a) shows the absorption coefficient (α) in the 350–1100 nm range, for all the tellurite glasses, together with the red-near-infrared Te^{4+} ($^3T_{1\,u} \rightarrow A_{1\,g}$ transition) PL spectrum, obtained by exciting the sample at 375 nm with a diode laser, and the PLE spectrum, from observing the emission at 620 nm, for the TL:Te^{4+}/0.6Ag glass. The absorption coefficient spectra for the TL:Te^{4+} and TL:Te^{4+}/0.6Ag glasses were similar, with some differences when compared to the spectrum for the TL:Te^{4+}/1.2Ag glass. The incorporation of 1.2 % of $AgNO_3$ in the glass caused a red shift of the UV absorption band, contributing to increased absorption in the UV region for this glass. Previous work has reported that the addition of AgNP can lead to a red shift of the glass absorption band in tellurite glass, mainly due to the effects of localized surface plasmon resonance [4].

The PLE spectrum (Fig. 2(a)) was normalized to coincide with the absorption spectrum at around 450 nm. The spectrum showed the well-known Te^{4+} absorption bands at 370 and 450 nm, corresponding to the transitions from $^1A_{1\,g}$ to $^3A_{1\,u}$ and from $^1A_{1\,g}$ to $^3T_{1\,u}$, respectively, as well as the broad red-near-infrared Te^{4+} emission band [15]. The Te^{4+} absorption bands overlapped with the AgNP absorption region and with the glass charge transfer band, as shown schematically in the partial energy diagram in Fig. 2(b). This indicated that when the glass system was excited at between around 300 and 500 nm, different absorption processes occurred simultaneously, so that the PL signal could only be from the Te^{4+} ion. For confirmation, a comparison was made among the excitation and emission profiles for all the glasses.

The optical behavior of our silver-containing samples provides strong evidence for the formation of silver nanoparticles (AgNPs) within the tellurite glass matrix. The characteristic red shift observed in the UV absorption band with increasing $AgNO_3$ content (Fig. 2a) is a recognized signature of localized surface plasmon resonance (LSPR) from metallic nanoparticles. This spectroscopic feature, combined with the preserved glass transparency (indicating structures significantly smaller than visible wavelengths) and the enhanced Te^{4+} emission without structural modification (as confirmed by our Raman analysis), strongly supports the presence of AgNPs. These findings align with previous studies of silver-doped tellurite glasses where silver nanoparticle formation was directly confirmed through TEM. [26] The AgNP formation likely occurs during the glass melting process, where the high temperature reduces Ag^+ ions to Ag^0, followed by nucleation and growth of nanoparticles

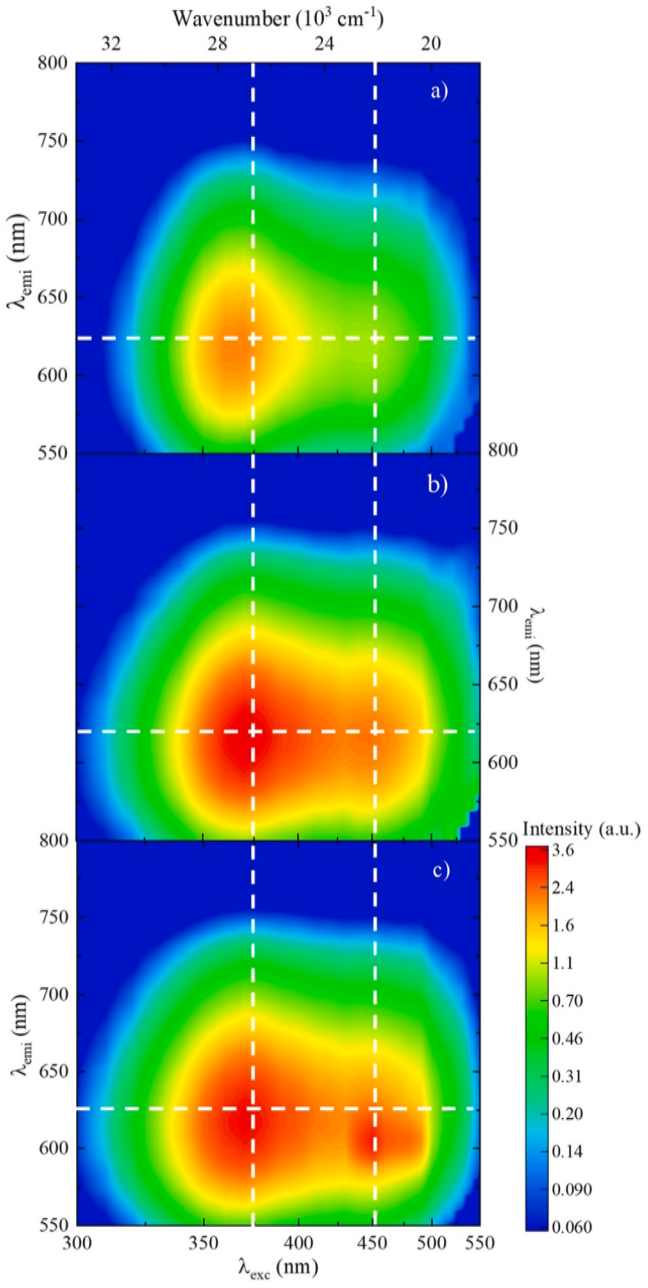

Fig. 3. Contour plot excitation-emission maps for the **(a)** TL:Te^{4+}, **(b)** TL:Te^{4+}/0.6Ag, and **(c)** TL:Te^{4+}/1.2Ag glasses, obtained using 300–550 nm excitation wavelength range and 525–800 nm emission observation range. The maximum intensity is represented by red and the minimum by blue.

during controlled cooling. The systematic increase in Te^{4+} emission with silver content provides further evidence of plasmonic enhancement effects characteristic of metal nanoparticles rather than isolated silver ions.

Fig. 3 shows excitation-emission contour plots for the glasses, using the same intensity scale range. The dashed white lines indicate the two main absorption positions (vertical lines) and the emission center (horizontal line) of Te^{4+}. The shapes and intensities of the two broad excitation bands changed with the incorporation of AgNP. As reported in the literature, AgNP added to the glass can contribute to the absorption in the UV-Vis region, with the maximum position being strongly dependent on AgNP size [37]. Another important finding was that the emission profile was the same for all the samples, with the maximum PL signal presenting a correlation with the Ag concentration. The

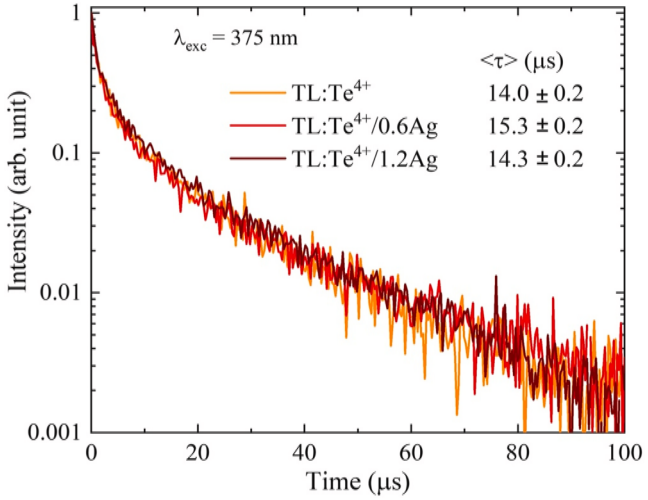

Fig. 4. Temporal dependence of Te^{4+} photoluminescence for the studied tellurite glasses, recorded at 620 nm, with excitation at 375 nm. The inset shows the average lifetime value for each glass.

enhancement of Te^{4+} emission intensity in the AgNP-containing glasses can be attributed to several established mechanisms. First, the localized surface plasmon resonance (LSPR) of AgNPs generates strong local electromagnetic fields that increase the absorption cross-section of nearby Te^{4+} ions, enhancing their excitation efficiency. This mechanism has been well-documented in various rare-earth doped glass systems. [38,39] s, The spectral overlap between the AgNP plasmon band and Te^{4+} absorption bands (~370–450 nm) enable efficient energy transfer from the AgNPs to the Te^{4+} ions, similar to what has been observed between AgNPs and other luminescent centers in glass hosts. [40] Third, AgNPs can modify the radiative decay rates of nearby Te^{4+} ions by altering the local dielectric environment, which is consistent with our observations that emission intensity increases significantly while lifetime values remain relatively unchanged. Furthermore, a significant factor facilitating the plasmon-ion interaction in our system is the chemical reaction occurring during the glass synthesis with $AgNO_3$. The added Ag^+ ions react with some of the Te^{3+} ions present in the base glass network via a redox process: $Ag^+ + Te^{3+} \rightarrow Ag^\circ + Te^{4+}$. This reaction produces metallic silver (Ag°), which aggregates into AgNPs, and simultaneously converts Te^{3+} into Te^{4+}. This process inherently places the forming AgNPs in close proximity to the newly created Te^{4+} ions, thus maximizing the potential for efficient LSPR field enhancement and plasmon-to-ion energy transfer. This reaction also contributes to the overall concentration of Te^{4+} ions in the glass.

The experimental observations described above support these enhancement mechanisms and the facilitated interaction due to synthesis: (1) the strong correlation between increasing AgNP concentration and Te^{4+} emission intensity; (2) the clear spectral overlap between AgNP absorption and Te^{4+} excitation bands as shown in Figs. 2 and 3; (3) the consistent emission profile of Te^{4+} across all samples regardless of AgNP content, indicating that the Te^{4+} emission mechanism itself remains unaltered; and (4) the modest changes in emission lifetime despite significant increases in emission intensity. These observations are consistent with plasmonic enhancement effects reported in other metal nanoparticle-luminescent ion systems. [26]

For each sample, the time dependence of the Te^{4+} emission was measured by exciting at 375 nm and observing the emission at 620 nm ($^3T_{1u} \rightarrow {}^1A_{1g}$ transition of Te^{4+}). The curves obtained for the emission intensity ($I(t)$) (Fig. 4) showed the expected non-exponential behavior, so the average lifetime, $\langle\tau\rangle$, could be calculated using the relation $\langle\tau\rangle = \int t\, I(t)\, dt / \int I(t)\, dt$ [41]. The experimentally determined average lifetimes (shown inset in Fig. 4) are characteristic of a relatively slow luminescence process. This longer decay time indicates a spin-forbidden

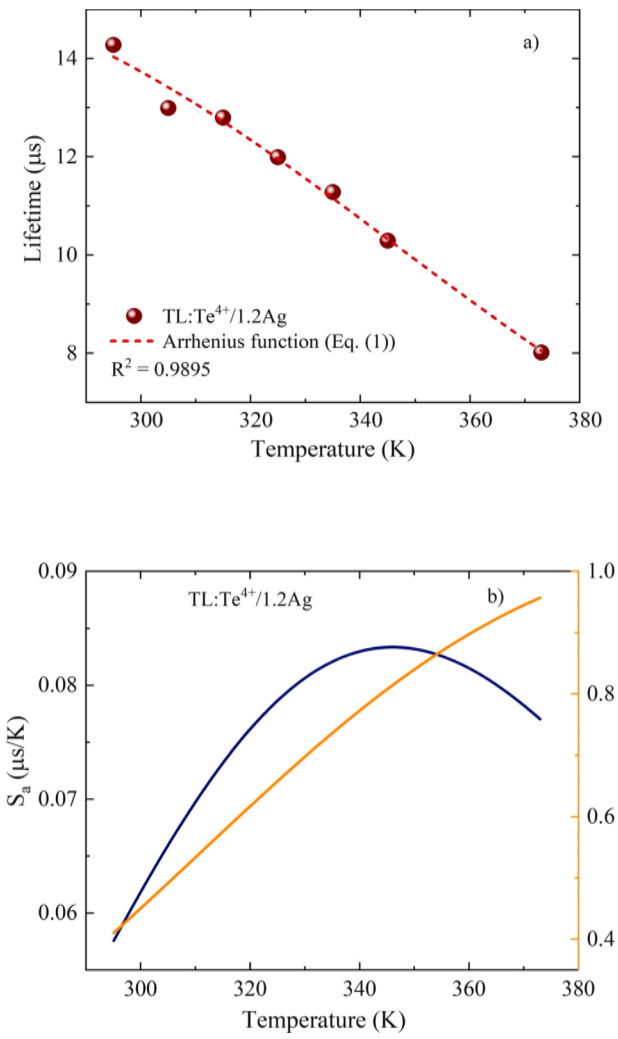

Fig. 5. (a) Temperature dependence of the Te^{4+} photoluminescence average lifetime for the TL:Te^{4+}/1.2Ag tellurite glass, recorded at 650 nm, with excitation at 375 nm. **(b)** Absolute (S_a) and relative (S_r) sensitivities calculated from the average measured lifetime values, according to Eq. 2(a) and 2(b), respectively.

transition from the triplet excited state to the singlet ground state of the Te^{4+} luminescence center, as such transitions are quantum mechanically restricted. The observed spectroscopic behavior, including this decay constant and the emission profile, aligns with the well-documented luminescence patterns of ns^2-type emission centers in oxide glass matrices. This is consistent with the electronic configuration of Te^{4+}, which has a $5\,s^2$ ground state configuration. The presence of these characteristic emission properties in our tellurium-doped oxide glasses demonstrate that Te^{4+} cations can function as effective luminescent centers.

The values obtained (shown in Fig. 4) indicated that the average lifetime for the TL:Te^{4+}/0.6Ag glass was only 9.0 % higher than for the other glasses, which presented similar $<\tau>$ values. Another point to note is that the values obtained were higher than those reported in the literature for Te^{4+}-doped zinc-borate glasses [17,42]. Although the PL maximum signal at 620 nm increased approximately twice with Ag dopant, as noted in Fig. 3, the Te^{4+} lifetime values were hardly affected, providing further evidence that different mechanisms acted in promoting the electron in Te^{4+}, without affecting the luminescence process.

Unlike traditional rare-earth doped tellurite glasses, the Te^{4+} luminescence in our system originates from the $5\,s^2$ electronic configuration of tellurium ions in the glass network itself. This ns^2 configuration creates a unique situation where concentration quenching is minimized even at high Te^{4+} concentrations due to three key factors: (1) the Te^{4+} ions are integral structural components of the glass network rather than dopants, resulting in a more uniform distribution that reduces ion-ion interactions that typically cause quenching; (2) the high polarizability of the tellurite glass matrix creates local environments that shield Te^{4+} centers from one another; and (3) the significantly different structures of TeO_3 and TeO_4 units in the glass network create multiple distinct Te^{4+} environments with slightly different emission energies, further reducing the probability of self-absorption. The non-exponential decay behavior observed in our samples reflects this structural heterogeneity, with Te^{4+} ions occupying different local environments within the glass network, each with slightly different decay rates. This heterogeneity, combined with the spin-forbidden nature of the $^3T_{1u} \rightarrow {}^1A_{1a}$ transition, explains both the microsecond-scale lifetime and the non-exponential decay profile observed in our measurements.

The detailed spectroscopic characterization of the samples indicated their suitability for testing as optical sensors for temperature measurements. Therefore, experiments were performed with insertion of the samples in a furnace controlled at different temperatures. The three

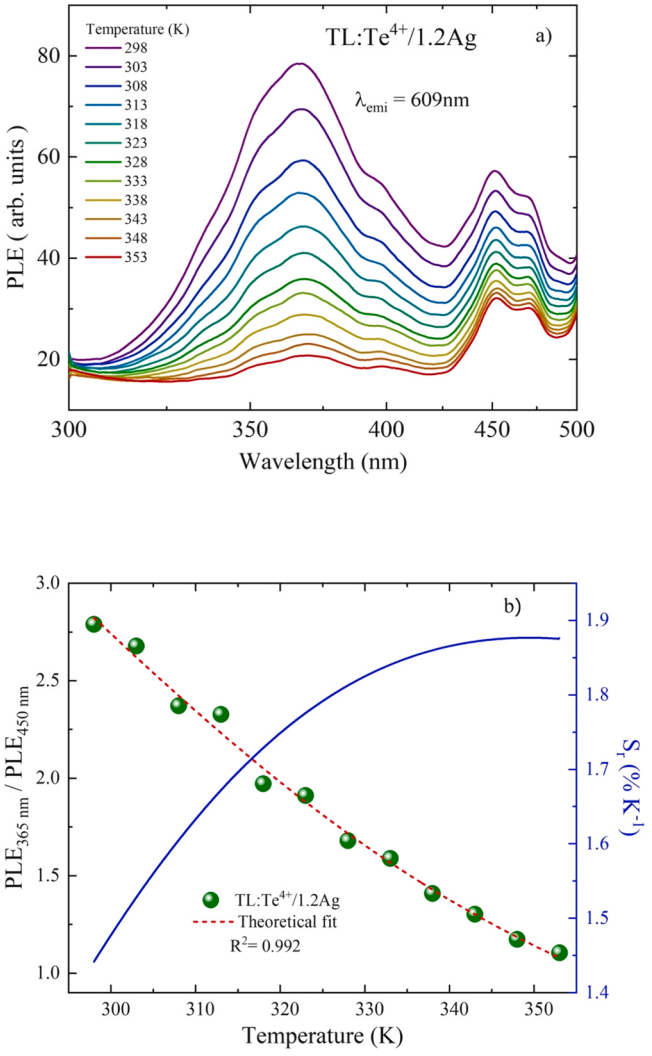

Fig. 6. (a) Photoluminescence excitation spectra, according to temperature, observing the Te^{4+} emission at 609 nm. **(b)** Photoluminescence excitation intensity at 365 nm normalized by the signal recorded at 450 nm ($PLE_{365\ nm}$/$PLE_{450\ nm}$ ratio), as a function of temperature (green spheres), together with the fitted curve obtained using the Arrhenius model (dashed red line) and relative sensitivity (solid blue line) determined using the experimental data and Eq. 2(b).

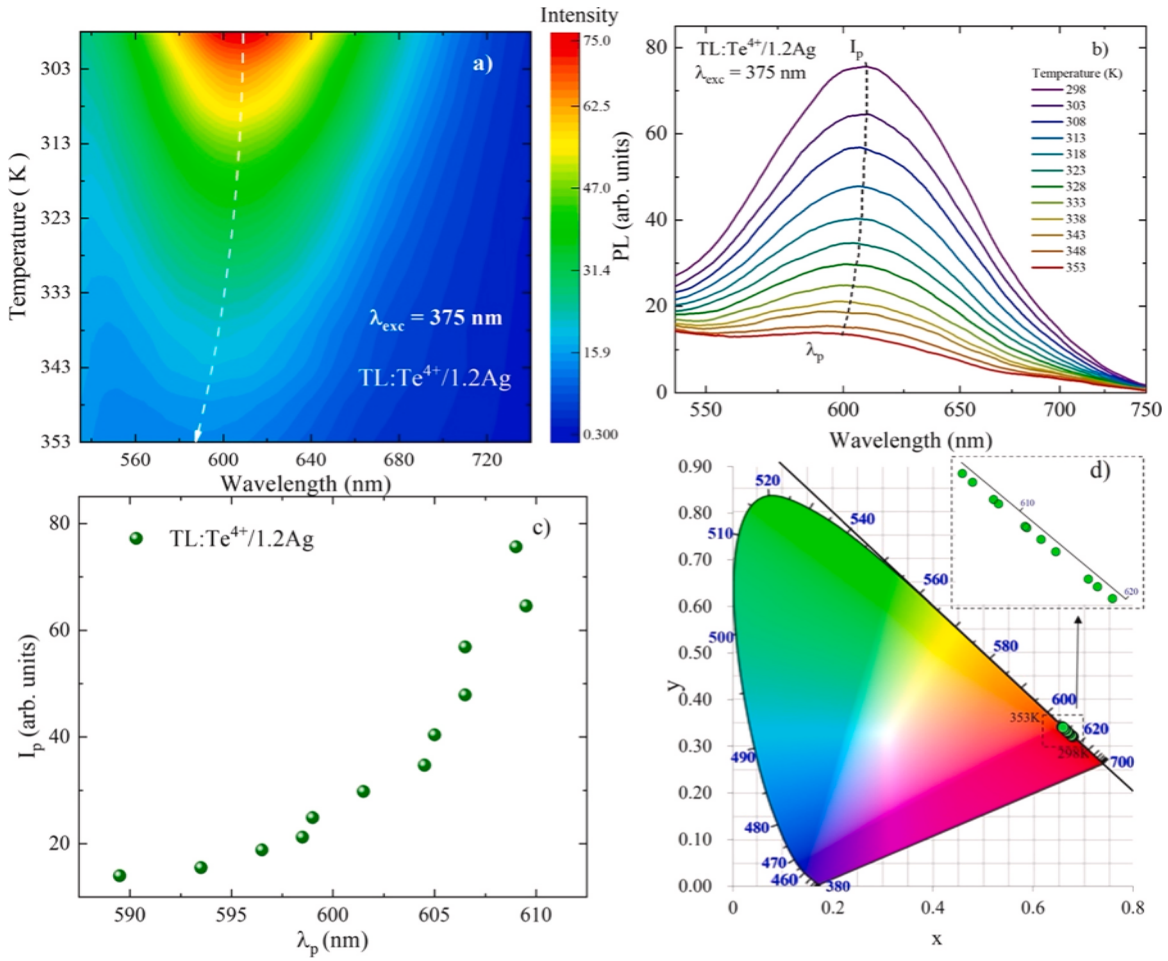

Fig. 7. **(a)** Color map of the Te^{4+} PL temperature dependence and **(b)** Te^{4+} PL spectra obtained with excitation at 375 nm, for the TL:Te^{4+}/1.2Ag glass. **(c)** Maximum PL intensity (I_p) according to the wavelength corresponding to the peak emission (λ_p). **(d)** CIE 1931 x-y coordinates for each spectrum.

different tests performed are described below.

3.3. Temperature sensing based on photoluminescence lifetime

The TL:Te^{4+}/1.2Ag glass was selected to study the temperature dependence of the PL lifetime. The average lifetime values (Fig. 5(a)) were determined by fitting the experimental curves (as described in Section 3.2). In the temperature interval evaluated, there was a decrease from 14.2 to 8.0 μs, with uncertainty less than 1 % for the used experimental setup. The average lifetime can be described using the Arrhenius model [7]:

$$\tau(T) = \frac{\tau_o}{1 - Ce^{-(\Delta E/k_B T)}} \quad (1)$$

where, τ_o is the emission lifetime when the temperature, T, is close to 0 K; C is a characteristic rate constant for the analyzed material; k_B is the Boltzmann constant (1.38×10^{-23} J/K = 0.695 cm^{-1}/K); and ΔE is the activation energy for thermal quenching. Using Eq. (1) to fit the experimental data in Fig. 5(a), the values obtained were $\tau_o = 21.9$ μs and $\Delta E = \sim 1840$ cm^{-1} ($R^2 = 0.9895$), which was only ~2.3 times the glass phonon energy (~800 cm^{-1}). This indicated thermal coupling among Te^{4+}-Te^{4+} pairs and Te^{4+} in the glassy network.

The performance of the TL:Te^{4+}/1.2Ag glass as a temperature sensor was evaluated by calculation of the absolute sensitivity (S_a) and the relative sensitivity (S_r), as follows [43]:

$$S_a = \left|\frac{dy}{dT}\right| \quad (2(a))$$

$$S_r = \frac{1}{y}\left|\frac{dy}{dT}\right| \times 100\% \quad (2(b))$$

where, y is the optical response recorded as a function of temperature, corresponding to the average lifetime determined by fitting Fig. 5(a) using the Arrhenius equation (Eq. 1). Fig. 5(b) shows the values of S_a and S_r obtained in the studied temperature range. The maximum calculated values for S_a and S_r were 0.083 μs/K at 345 K and 0.95 %/K at around 370 K, respectively, which could be considered a very good result for a tellurite glass that was not doped with a rare earth.

3.4. Photoluminescence excitation intensity ratio for temperature sensing

PLE spectra for the TL:Te^{4+}/1.2Ag glass were obtained at different temperatures, observing the emission at 609 nm. As shown in Fig. 6(a), there was a non-uniform decrease in the PLE intensity, comparing the signals at around 370 and 450 nm, with the Te^{4+} emission being less affected by temperature for absorption at 450 nm, compared to absorption at 370 nm. The observed behavior suggested that the AgNP effectively contributed to the absorption at 450 nm. This was also evidenced by the excitation-emission color maps (Fig. 3).

To calculate S_r for these experimental data, the PLE spectra were deconvoluted using 6 Gaussian curves, to obtain the ratios of the areas centered at 365 and 450 nm, as a function of temperature. The data obtained (Fig. 6(b)) were fitted by an expression equivalent to Eq. (1), with $R^2 = 0.992$. From the parameters obtained with the fit shown in Fig. 6(b), an experimental curve (defined as y in Eq. 2(b)) was obtained

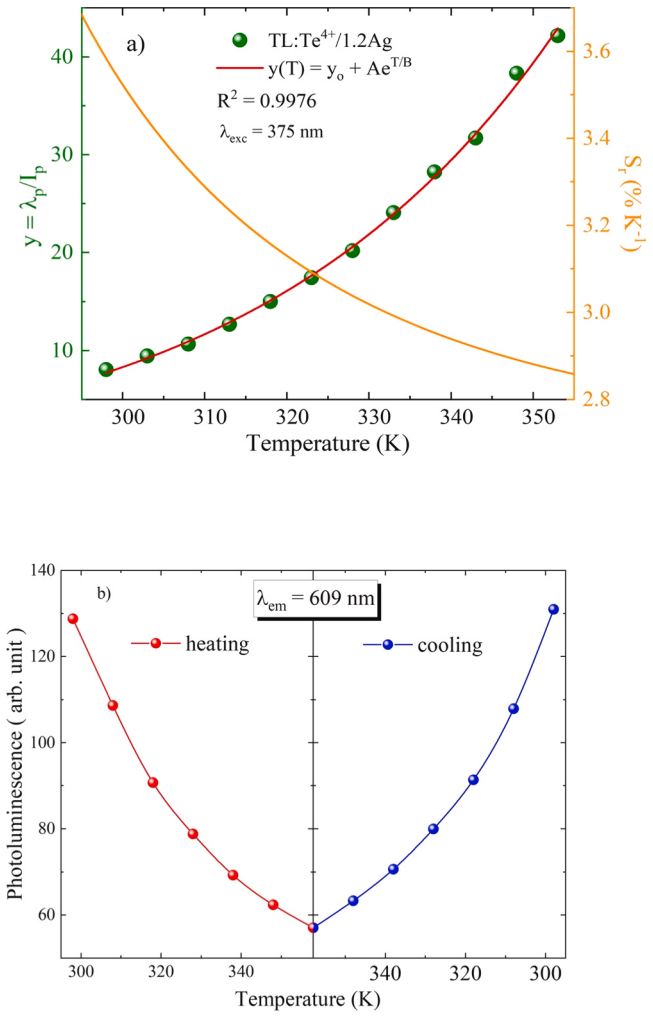

Fig. 8. (a) λ_p/I_p ratio (green spheres) and relative sensitivity (S_r, orange line), as a function of temperature, for the TL:Te^{4+}/1.2Ag glass. **(b)** PL intensity, as a function of temperature, during heating and cooling.

to determine S_r, as also shown in Fig. 6(b). Irrespective of the temperature, S_r was higher than unity, with a maximum value (~1.75 %/K) recorded above 345 K. This result indicated that the use of PLE with this glass system could be an important methodology for an optical temperature sensor, showing better relative sensitivity than the lifetime observation described in Section 3.3.

3.5. Photoluminescence intensity ratio for temperature sensing

The 375 nm emission from a Xe lamp was used to excite the sample, with recording of the PL spectrum from 525 to 750 nm, for each temperature. Fig. 7(a) shows the tri-dimensional PL plot, while Fig. 7(b) shows the related spectra for each 5 K from 298 to 353 K. These results clearly showed that as the temperature increased, the peak Te^{4+} emission intensity (I_p) decreased (by ~83 %), while the corresponding wavelength position of the peak (λ_p) presented a blue shift. A possible explanation for this shift was the presence of self-trapped excitons (STEs) resulting from lattice vibrations of the distorted structures in the glass [[44]. This was recently reported for cesium zinc chloride crystal doped with Te^{4+}, where structures with some deformation (as occurs in tellurite glasses) facilitate STE formation [45]. Fig. 7(c) shows a plot of I_p against λ_p, indicating a nonlinear correlation between these optical parameters, so they could be used to calculate S_r for the optical temperature sensor.

To better observe the temperature dependence of λ_p, the PL spectra were deconvoluted using the three-color matching functions established by the Commission Internationale de l'Éclairage (CIE) in 1931. The calculated (x, y) coordinates are plotted in Fig. 7(d), showing that the maximum position of λ_p changed in the red range, with the correlated color temperature (CCT) shifting from 2700 to 3860 K, when the sample temperature was increased from 298 to 353 K.

The λ_p/I_p ratio values could then be used to determine S_r, according to Eq. 2(b) (here, $y = \lambda_p/I_p$). Fig. 8(a) shows a plot of the λ_p/I_p values against temperature, together with the curve fit obtained using a theoretical exponential equation of the type $y(T) = y_o + Ae^{B/T}$. From the fit ($R^2 = 0.9976$), a better curve could be obtained to determine S_r (also shown in Fig. 8(a)). Maximum S_r was around 3.7 %/K at room temperature, while the minimum was 2.85 %/K at 360 K. The maximum S_r value was slightly higher than obtained for a Rb_2ScCl_5:H_2O:0.1 %Te^{4+} single crystal (3.53 %/K) by monitoring the fluorescence lifetime-temperature dependence, [45] as well as higher than reported for tellurite glasses doped with different rare earths [8,46].

Recently our group explored the optical properties of a Nd^{3+}-doped Tellurite glass for fluorescence infrared thermometry. The obtained results indicated a very high sensitivity (3.00 %/K) at 370 K, highlighting the tellurite glass when compared with other glass families [8].

The stability of the TL:Te^{4+}/1.2Ag glass was evaluated using PL measurements as a function of temperature, during a complete cycle between 300 and 360 K. The maximum emission intensity remained similar after a heating/cooling cycle, as shown in Fig. 8(b) for the PL signal at 609 nm recorded at different temperatures. Similar experimental procedures were also performed for the temperature sensing based on the photoluminescence lifetime (described on Section 3.3) and based on the photoluminescence excitation intensity (Section 3.4), indicating the same very good reproducibility shown in Fig. 8(b).

This third methodology using the tellurite glass as an optical temperature sensor provided a higher maximum S_r value, compared to the two preceding methods. To investigate the dependence of S_r on the $AgNO_3$ concentration, the same methodology described here was also applied with the TL:Te^{4+} and TL:Te^{4+}/0.6Ag glasses, resulting in maximum S_r values of 1.86 and 0.66 %/K, respectively, at room temperature. A glass with 2.4 % of $AgNO_3$ was also prepared for testing as an optical temperature sensor, with no observed improvement, so the present results highlighted the TL:Te^{4+}/1.2Ag glass as a potential candidate for use in optical temperature sensing applications.

4. Conclusions

In this study, investigation was made of the effects of AgNP on the structure and Te^{4+} photoluminescence of a tellurite glass. The glass material was evaluated as an optical sensor for temperatures between 298 and 370 K, employing three different methods: (1) monitoring the average emission lifetime, which provided maximum relative sensitivity (S_r) of 0.95 %/K; (2) measuring the Te^{4+} photoluminescence excitation, observing the emission at 609 nm, with maximum S_r of ~1.75 %/K; (3) calculation of S_r using the ratio of the maximum emission intensity and the wavelength corresponding to the peak position, with maximum S_r of 3.7 %/K at room temperature. Method (2) is a novel way to use photoluminescence excitation spectroscopy to measure temperature, enabling simpler operation of the device, since two independent excitations (at 375 and 450 nm) can be used to record the PL intensity (at 609 nm), while method (3) provides greater relative sensitivity. Compared to other ions with similar electronic configurations, Te^{4+} doped tellurite glass exhibits the significant advantage to present high luminescence quantum efficiency. Furthermore, this glass possesses a broad emission band, enabling the selection of the optimal wavelength for temperature-dependent emission monitoring. The excitation band of Te^{4+} in this glass is also broad, providing flexibility in choosing a convenient and cost-effective pump source. Moreover, the strong temperature dependence of Te^{4+} luminescence endows the tellurite glass with high sensitivity, making it a promising candidate for optical

temperature sensing applications, what can be noted by the excellent performance of this tellurite glass when compared to materials reported previously in the literature.

CRediT authorship contribution statement

Adriana do Carmo Capiotto: Data curation, Investigation, Methodology, Formal Analysis, Writing – original draft. **Junior Reis Silva:** Conceptualization, Investigation, Methodology, Formal Analysis, Writing – original draft. **Luiz Anotnio de Oliveira Nunes:** Conceptualization, Investigation, Methodology **Luis H. C. Andrade:** Visualization, Writing- review and editing. **Sandro M. Lima:** Conceptualization, Project Administration, Investigation, Methodology, Supervision, Validation, Writing- review and editing.

Declaration of Competing Interest

The authors declare the following financial interests/personal relationships which may be considered as potential competing interests: Sandro Marcio Lima reports financial support was provided by National Council for Scientific and Technological Development. SANDRO MARCIO LIMA reports a relationship with Coordination of Higher Education Personnel Improvement that includes: funding grants. SANDRO MARCIO LIMA has patent #SENSOR DE TEMPERATURA ÓPTICO BASEADO NA EMISSÃO DE ÍONS TE4 + PRESENTES EM VIDRO TELURITO DOPADO COM NANOPARTÍCULA DE PRATA pending to BR 10 2023 027916 3. If there are other authors, they declare that they have no known competing financial interests or personal relationships that could have appeared to influence the work reported in this paper.

Acknowledgments

Financial support for this work was provided by Coordenação de Aperfeiçoamento de Pessoal de Nível Superior (CAPES, #00889834/0001–08), Conselho Nacional de Desenvolvimento Científico e Tecnológico (CNPq, grant to S.M.L.: #307436/2023–3; J.R.S.: #308242/2022–0; L.H.C.A.: #303707/2022-4), and Fundação de Apoio ao Desenvolvimento do Ensino, Ciência e Tecnologia do Estado de Mato Grosso do Sul (FUNDECT, #71/023.765/2021).

Data availability statement

The data that support the findings of this study are available from the corresponding author upon reasonable request.

References

[1] Q. Ma, Q. Liu, M. Wu, Y.L.R. Wang, R. Zhou, Y. Xu, H. Wei, R. Mi, X. Min, L. Mei, Z. Huang, B. Ma, Eu^{3+}-doped $La_2(MoO_4)_3$ phosphor for achieving accurate temperature measurement and non-contact optical thermometers, Ceram. Int. 49 (2023) 8204–8211, https://doi.org/10.1016/j.ceramint.2022.10.345.

[2] K. Trejgis, R. Lisiecki, A. Bednarkiewicz, L. Marciniak, Nd^{3+} doped TZPN glasses for NIR operating single band ratiometric approach of contactless temperature readout, J. Lumin 224 (2020), https://doi.org/10.1016/j.jlumin.2020.117295.

[3] T. Zhao, G. Chen, Te^{4+} doped Cs_2ZrCl_6 perovskite for optical temperature sensing at low temperature, Opt. Mater. 136 (2023), https://doi.org/10.1016/j.optmat.2022.113355.

[4] G.S. Bezerra, L.R. Ocas, D. Kendji Kumada, W.S. Martins, L.R.P. Kassab, A.S. Reyna, Influence of plasmonic and thermo-optical effects of silver nanoparticles on near-infrared optical thermometry in Nd^{3+}-doped TeO_2–ZnO glasses, J. Lumin 265 (2024), https://doi.org/10.1016/j.jlumin.2023.120222.

[5] H. Xu, J. Yu, Q. Hu, Q. Han, W. Wu, Highly sensitive Dual-Mode optical thermometry of Er^{3+}/Yb^{3+}Codoped Lead-Free double perovskite microcrystal, J. Phys. Chem. Lett. 13 (2022) 962–968, https://doi.org/10.1021/acs.jpclett.1c04000.

[6] D. Chen, Z. Wan, Y. Zhou, Optical spectroscopy of Cr^{3+}-doped transparent nano-glass ceramics for lifetime-based temperature sensing, Opt. Lett. 40 (2015) 3607, https://doi.org/10.1364/ol.40.003607.

[7] L.-K. Wu, H.-Y. Sun, L.-H. Li, R.-F. Li, H.-Y. Ye, J.-R. Li, Te^{4+}-Doping rubidium scandium halide perovskite single crystals enabling optical thermometry, J. Phys. Chem. C 126 (2022) 21689–21698, https://doi.org/10.1021/acs.jpcc.2c07553.

[8] C.Y. Morassuti, A.P. L Silva, L.A.O. Nunes, S.M. Lima, L.H.C. Andrade, Effect of radiative loss mechanisms on FIR thermometric parameters of Nd^{3+}-doped lithium tellurite glasses, J. Rare Earth 42 (2024) 1250–1257, https://doi.org/10.1016/j.jre.2023.06.004.

[9] C.Y. Morassuti, L.A.O. Nunes, S.M. Lima, L.H.C. Andrade, Eu^{3+}-doped alumino-phosphate glass for ratiometric thermometer based on the excited state absorption, J. Lumin 193 (2018) 39–43, https://doi.org/10.1016/j.jlumin.2017.09.001.

[10] S. Li, Q. Meng, S. Lü, W. Sun, Optical properties of Sm^{3+} and Tb^{3+} co-doped $CaMoO_4$ phosphor for temperature sensing, Spectrochim. Acta A Mol. Biomol. Spectrosc. 214 (2019) 537–543, https://doi.org/10.1016/j.saa.2019.02.049.

[11] I.E. Kolesnikov, A.A. Kalinichev, M.A. Kurochkin, D.V. Mamonova, E. Y. Kolesnikov, A.V. Kurochkin, E. Lähderanta, M.D. Mikhailov, New strategy for thermal sensitivity enhancement of Nd^{3+}-based ratiometric luminescence thermometers, J. Lumin 192 (2017) 40–46, https://doi.org/10.1016/j.jlumin.2017.06.024.

[12] K. Trejgis, K. Maciejewska, A. Bednarkiewicz, L. Marciniak, Near-Infrared-to-Near-Infrared Excited-State absorption in $LaPO_4$:Nd^{3+} nanoparticles for luminescent nanothermometry, ACS Appl. Nano Mater. 3 (2020) 4818–4825, https://doi.org/10.1021/acsanm.0c00853.

[13] J. Drabik, R. Kowalski, L. Marciniak, Enhancement of the sensitivity of single band ratiometric luminescent nanothermometers based on Tb^{3+} ions through activation of the cross relaxation process, Sci. Rep. 10 (2020), https://doi.org/10.1038/s41598-020-68145-5.

[14] El-Mallawany R.A.H., Tellurite Glasses Handbook, Boca Raton, 2012. https://doi.org/https://doi.org/10.1201/b11295.

[15] F.B. Costa, A.K.R. Souza, A.P. Langaro, J.R. Silva, F.A. Santos, M.S. Figueiredo, K. Yukimitu, J.C.S. Moraes, L.A.O. Nunes, L.H.C. Andrade, S.M. Lima, Observation of a Te^{4+} center with broad red emission band and high fluorescence quantum efficiency in TeO_2-Li_2O glass, J. Lumin 198 (2018) 24–27, https://doi.org/10.1016/j.jlumin.2018.02.002.

[16] B.C. Lima, L.A. Gómez-Malagón, A.S.L. Gomes, J.A.M. Garcia, L.R.P. Kassab, Plasmon-Assisted efficiency enhancement of Eu^{3+}-Doped tellurite Glass-Covered solar cells, J. Electron Mater. 46 (2017) 6750–6755, https://doi.org/10.1007/s11664-017-5744-x.

[17] H. Masai, T. Yanagida, Photoluminescence of ns^2-type center-containing zinc borate glasses, J. Non Cryst. Solids 431 (2016) 83–87, https://doi.org/10.1016/j.jnoncrysol.2015.03.029.

[18] T. Sekiya, N. Mochida, A. Ohtsuka, M. Tonokawa, Raman spectra of $MO_{1/2}$-TeO_2 (M = Li, Na, K, Rb, Cs and Tl), J. Non-Cryst. Solids 144 (1992) 128–144, https://doi.org/10.1016/S0022-3093(05)80393-X.

[19] T. Sekiya, N. Mochida, A. Soejima, Raman spectra of binary tellurite glasses containing tri- or tetra-valent cations, J. Non Cryst. Solids 191 (1995) 115–123, https://doi.org/10.1016/0022-3093(95)00290-1.

[20] A.K.R. Souza, J.R. Silva, F.B. Costa, J.C.S. Moraes, L.A.O. Nunes, L.H.C. Andrade, S. M. Lima, A systematic interpretation of the quantum cutting effect by a cooperative energy transfer mechanism in Te^{4+}/Yb^{3+} co-doped tellurite glasses, Ceram. Int. 49 (2023) 19470–19480, https://doi.org/10.1016/j.ceramint.2023.03.079.

[21] A.K.R. Souza, A.P. Langaro, J.R. Silva, F.B. Costa, K. Yukimitu, J.C.S. Moraes, L.A. O. Nunes, L.H.C. Andrade, S.M. Lima, On the efficient $Te^{4+}\rightarrow Yb^{3+}$ cooperative energy transfer mechanism in tellurite glasses: a potential material for luminescent solar concentrators, J. Alloy. Compd. (2019) 1119–1126, https://doi.org/10.1016/j.jallcom.2018.12.038.

[22] A. do, C. Capiotto, A.K.R. Souza, F.B. Costa, J.C.S. Moraes, L.A.O. Nunes, J.R. Silva, L.H.C. Andrade, S.M. Lima, Influence of synthesis temperature and atmosphere on Te^{4+} ion formation in lithium tellurite glass, Ceram. Int. 47 (2021) 32195–32201, https://doi.org/10.1016/j.ceramint.2021.08.112.

[23] L.R.P. Kassab, R. De Almeida, D.M. Da Silva, C.B. De Araújo, Luminescence of Tb^{3+} doped TeO_2-ZnO-Na_2O-PbO glasses containing silver nanoparticles, J. Appl. Phys. 104 (2008), https://doi.org/10.1063/1.3010867.

[24] M.R. Dousti, R.J. Amjad, Enhanced Green emission of terbium-ions-doped phosphate glass embedding metallic nanoparticles, J. Nanophoton. 9 (2015) 093068, https://doi.org/10.1117/1.jnp.9.093068.

[25] D.K. Kumada, M.S. Peixoto, L.A. Gomez-Malagon, R.K. Onmori, J.A.M. Garcia, L.R. P. Kassab, Influence of silver nanoparticles on Tb^{3+} doped TeO_2-ZnO glasses covered silicon solar cell, 34th Symp. Microelectron. Technol. Dev. (2019), https://doi.org/10.1109/SBMicro.2019.8919331.

[26] L.R.P. Kassab, R. De Almeida, D.M. Da Silva, T.A.A. De Assumpão, C.B. De Araújo, Enhanced luminescence of Tb^{3+}/Eu^{3+} doped tellurium oxide glass containing silver nanostructures, J. Appl. Phys. 105 (2009) 103505, https://doi.org/10.1063/1.3126489.

[27] I. Soltani, S. Hraiech, K. Horchani-Naifer, M. Férid, Effects of silver nanoparticles on the enhancement of up conversion and infrared emission in Er^{3+}/Yb^{3+} co-doped phosphate glasses, Opt. Mater. 77 (2018) 161–169, https://doi.org/10.1016/j.optmat.2018.01.036.

[28] P. Cheng, Y. Zhou, X. Su, M. Zhou, Z. Zhou, H. Shao, Pr^{3+}/Er^{3+} co-doped tellurite glass with ultra-broadband near-infrared fluorescence emission, J. Lumin. 197 (2018) 31–37, https://doi.org/10.1016/j.jlumin.2018.01.005.

[29] J. Heo, D. Lam, G.H. Sigel, E.A. Mendoza, D.A. Hensley, Spectroscopic analysis of the structure and properties of alkali tellurite glasses, J. Am. Ceram. Soc. 75 (1992) 277–281, https://doi.org/10.1111/j.1151-2916.1992.tb08176.x.

[30] C.R. Kesavulu, V.B. Sreedhar, C.K. Jayasankar, K. Jang, D.S. Shin, S.S. Yi, Structural, thermal and spectroscopic properties of highly Er^{3+}-doped novel oxyfluoride glasses for photonic application, Mater. Res. Bull. 51 (2014) 336–344, https://doi.org/10.1016/j.materresbull.2013.12.023.

[31] V. Sreenivasulu, G. Upender, Swapna, V.V. Priya, V.C. Mouli, M. Prasad, Raman, DSC, ESR and optical properties of lithium cadmium zinc tellurite glasses, Phys. B Condens Matter 454 (2014) 60–66, https://doi.org/10.1016/j.physb.2014.06.039.
[32] A.K. Yadav, P. Singh, A review of structure of oxide glasses by Raman spectroscopy, RCS Adv. 5 (83) (2015) 67583–67609, https://doi.org/10.1039/c0xx00000x.
[33] E.R. Barney, A.C. Hannon, D. Holland, N. Umesaki, M. Tatsumisago, R.G. Orman, S. Feller, Terminal oxygens in amorphous TeO_2, J. Phys. Chem. Lett. 4 (2013) 2312–2316, https://doi.org/10.1021/jz4010637.
[34] A. Kaur, A. Khanna, F. González, C. Pesquera, B. Chen, Structural, optical, dielectric and thermal properties of molybdenum tellurite and borotellurite glasses, J. Non Cryst. Solids 444 (2016) 1–10, https://doi.org/10.1016/j.jnoncrysol.2016.04.033.
[35] A. Kaur, A. Khanna, L.I. Aleksandrov, Structural, thermal, optical and photoluminescent properties of barium tellurite glasses doped with rare-earth ions, J. Non Cryst. Solids 476 (2017) 67–74, https://doi.org/10.1016/j.jnoncrysol.2017.09.025.
[36] N. Gupta, A. Kaur, A. Khanna, F. Gonzàlez, C. Pesquera, R. Iordanova, B. Chen, Structure-property correlations in TiO_2-Bi_2O_3-B_2O_3-TeO_2 glasses, J. Non Cryst. Solids 470 (2017) 168–177, https://doi.org/10.1016/j.jnoncrysol.2017.05.021.
[37] M.M. Martins, L.R.P. Kassab, D.M. da Silva, C.B. de Araújo, Tm^{3+} doped Bi_2O_3-GeO_2 glasses with silver nanoparticles for optical amplifiers in the short-wave-infrared-region, J. Alloy. Compd. 772 (2019) 58–63, https://doi.org/10.1016/j.jallcom.2018.08.146.
[38] V.A.G. Rivera, S.P.A. Osorio, 2 D. Manzani, Y. Ledemi, Y. Messaddeq, L.A. O. Nunes, E. Marega Jr., Localized surface plasmon resonance interaction with Er^{3+}-doped tellurite glass, Opt. Express 18 (2010) 25321–25328, https://doi.org/10.1364/OE.18.025321.
[39] H. Fares, H. Elhouichet, B. Gelloz, M. Férid, Silver nanoparticles enhanced luminescence properties of Er^{3+} doped tellurite glasses: effect of heat treatment, J. Appl. Phys. 116 (2014) 123504, https://doi.org/10.1063/1.4896363.
[40] J. Li, R. Wei, X. Liu, H. Guo, G. Blasse, B.C. Grabmaier, L.M. Springer, F. Wang, R. Deng, J. Wang, Q. Wang, Y. Han, H. Zhu, X. Chen, X. Liu, Enhanced luminescence via energy transfer from Ag^+ to RE ions (Dy^{3+}, Sm^{3+}, Tb^{3+}), Opt. Express 20 (9) (2012) 10122–10127, https://doi.org/10.1364/OE.20.010122.
[41] J.R. Lakowicz, Principles of Fluorescence Spectroscopy, Springer, 2006. ⟨https://link.springer.com/book/10.1007/978-0-387-46312-4⟩.
[42] H. Masai, Y. Yamada, S. Okumura, Y. Kanemitsu, T. Yoko, Photoluminescence of a Te^{4+} center in zinc borate glass, Opt. Lett. 38 (2013) 3780, https://doi.org/10.1364/ol.38.003780.
[43] B.J. Guild, The colorimetric properties of the spectrum, R. Soc. 230 (1931) 681–693, https://doi.org/10.1098/rsta.1932.0005.
[44] S. Li, J. Luo, J. Liu, J. Tang, Self-Trapped excitons in All-Inorganic halide perovskites: fundamentals, status, and potential applications, J. Phys. Chem. Lett. 10 (2019) 1999–2007, https://doi.org/10.1021/acs.jpclett.8b03604.
[45] H. Yu, J. Liu, J. Zhang, S. Zhao, X. Li, W. Wu, Luminescence properties and optical thermometry behavior of Te^{4+}-doped cesium zinc chloride crystals, Ceram. Int. (2024), https://doi.org/10.1016/j.ceramint.2024.08.438.
[46] J. Stefanska, L. Marciniak, M. Chrunik, Sensitivity enhancement of the Tb^{3+}-based single band ratiometric luminescent thermometry by the metal-to-metal charge transfer process, J. Phys. Chem. C 125 (2021) 5226–5232, https://doi.org/10.1021/acs.jpcc.0c11631.